Title

Interplay between Two Bacterial Actin Homologs, MamK and MamK-Like, Is Required for the Alignment of Magnetosome Organelles in Magnetospirillum magneticum AMB-1

Journal

Journal of Bacteriology, 196(17)

ISSN

0021-9193

Authors

Abreu, Nicole
Mannoubi, Soumaya
Ozyamak, Ertan
et al.

Publication Date

2014-09-01

DOI

10.1128/jb.01674-14

Peer reviewed

JB
Journals.ASM.org

Interplay between Two Bacterial Actin Homologs, MamK and MamK-Like, Is Required for the Alignment of Magnetosome Organelles in *Magnetospirillum magneticum* AMB-1

Nicole Abreu,[a] Soumaya Mannoubi,[b,c,d] Ertan Ozyamak,[a] David Pignol,[b,c,d] Nicolas Ginet,[b,c,d] Arash Komeili[a]

Department of Plant and Microbial Biology, University of California, Berkeley, Berkeley, California, USA[a]; CEA, IBEB, Lab Bioenerget Cellulaire, Saint-Paul-lez-Durance, France[b]; CNRS, UMR Biol Veget & Microbiol Environ, Saint-Paul-lez-Durance, France[c]; Aix-Marseille Université, Saint-Paul-lez-Durance, France[d]

Many bacterial species contain multiple actin-like proteins tasked with the execution of crucial cell biological functions. MamK, an actin-like protein found in magnetotactic bacteria, is important in organizing magnetosome organelles into chains that are used for navigation along geomagnetic fields. MamK and numerous other magnetosome formation factors are encoded by a genetic island termed the magnetosome island. Unlike most magnetotactic bacteria, *Magnetospirillum magneticum* AMB-1 (AMB-1) contains a second island of magnetosome-related genes that was named the magnetosome islet. A homologous copy of *mamK*, *mamK-like*, resides within this islet and encodes a protein capable of filament formation *in vitro*. Previous work had shown that *mamK-like* is expressed *in vivo*, but its function, if any, had remained unknown. Though MamK-like is highly similar to MamK, it contains a mutation that in MamK and other actins blocks ATPase activity *in vitro* and filament dynamics *in vivo*. Here, using genetic analysis, we demonstrate that *mamK-like* has an *in vivo* role in assisting organelle alignment. In addition, MamK-like forms filaments *in vivo* in a manner that is dependent on the presence of MamK and the two proteins interact in a yeast two-hybrid assay. Surprisingly, despite the ATPase active-site mutation, MamK-like is capable of ATP hydrolysis *in vitro* and promotes MamK filament turnover *in vivo*. Taken together, these experiments suggest that direct interactions between MamK and MamK-like contribute to magnetosome alignment in AMB-1.

Despite their small size, bacterial cells are remarkably organized and can display a stunning degree of control over the production and positioning of highly ordered subcellular structures (1–3). Magnetotactic bacteria (MTB) are recognized for their ability to form organelles called magnetosomes (4). These compartments are derived from the inner cell membrane and, with the aid of specialized proteins, synthesize magnetic iron-based crystals. MTB align these individual magnetosomes into an ordered chain within the cell that provides navigational capability for movement toward preferred oxygen concentrations in stratified water columns (5). One such bacterium, *Magnetospirillum magneticum* AMB-1 (AMB-1), serves as an excellent model organism for examination of these cellular processes.

In most MTB, the genes required for magnetosome formation are carried in a genomic region called the magnetosome island (MAI). One of the magnetosome genes conserved in all MTB studied to date is *mamK*, which encodes a bacterial actin protein. The bacterial actin superfamily contains numerous phylogenetically distinct subgroups (6, 7), each of which includes members that participate in specialized functions such as cell shape determination (8–10), motility (11), DNA segregation (12–14), and cytokinesis (15, 16). High-resolution imaging of AMB-1 cells by electron cryotomography (ECT) shows that magnetosomes are flanked by filamentous structures (17). In AMB-1, the deletion of *mamK* results in a disorganized magnetosome chain and loss of magnetosome-associated filaments (17). *Magnetospirillum gryphiswaldense* MSR-1 (MSR-1), a close relative of AMB-1, appears to utilize MamK in a distinct manner to position its magnetosome chains within the cell (18). In stark contrast to AMB-1, MSR-1 magnetosome chains do not span the cell length and require magnetic interactions as well as MamK for their assembly. Furthermore, after cell division in MSR-1, magnetosome chains rapidly relocalize to the midcell of daughter cells in a process that seems to require MamK (18). However, since the magnetosome chain of AMB-1 spans the entire length of the cell, cell division-coupled relocalization of the magnetosome chain is not likely to occur. Additionally, MamK has been hypothesized to interact with signaling proteins in order to translate relative orientations in magnetic fields into changes in cell motility (19). Thus, while MamK is a central player in magnetosome chain organization, the specific mode of its action, its species-specific activities, and the full range of its cellular functions remain unknown.

Much like other actin-like proteins, MamK is able to polymerize and depolymerize in a manner that is dependent on its ATPase activity. ATP-bound MamK monomers assemble into filaments, and ATP hydrolysis is required for filament depolymerization *in vitro* (20). MamK filaments also require an intact ATPase active site and the action of other magnetosome proteins to exhibit dynamics *in vivo*. In particular, a highly acidic protein, MamJ, and its homolog LimJ are necessary for the dynamic behavior of MamK in AMB-1 (21). MamJ also participates in magnetosome chain formation since its deletion in MSR-1 results in a dramatic aggregation of magnetosomes within the cell (22). In AMB-1, the deletion of *mamJ* and *limJ* leads to a completely different phenotype,

Received 18 March 2014 **Accepted** 10 June 2014
Published ahead of print 23 June 2014
Address correspondence to Arash Komeili, komeili@berkeley.edu.
Supplemental material for this article may be found at http://dx.doi.org/10.1128/JB.01674-14.

doi:10.1128/JB.01674-14

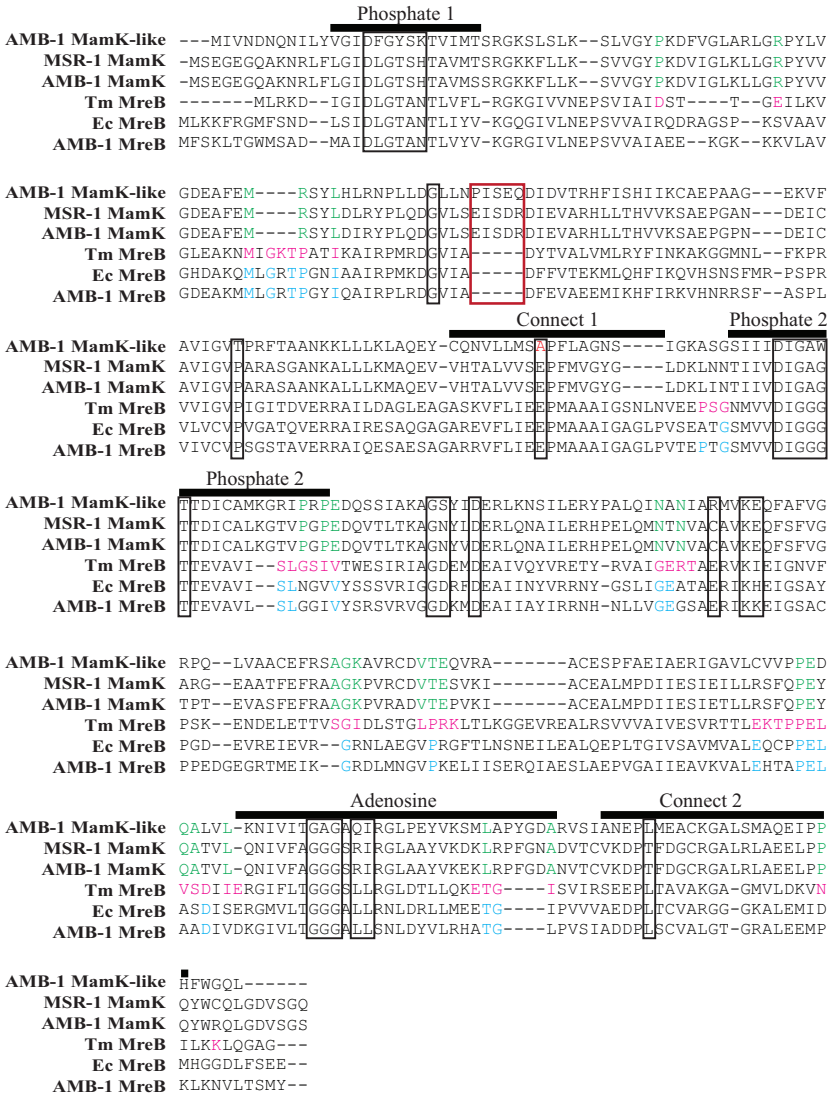

FIG 1 (A) Alignment of MamK-like, MamK, and MreB proteins. Highly conserved ATPase residues are boxed. MamK-like's A141 residue is marked red. Potential monomer-monomer interaction residues within the MreB protofilament are marked pink (40). Residues conserved between MamK and MamK-like in these regions are marked green. Residues conserved between MreB proteins in these regions are marked blue. Alignment was generated with MUSCLE. (AMB-1, *Magnetospirillum magneticum* AMB-1; MSR-1, *Magnetospirillum gryphiswaldense* MSR-1; Tm, *Thermotoga maritima*; Ec, *Escherichia coli*.)

with the appearance of a few gaps in the magnetosome chain (21). The differences between the chain organization phenotypes of *mamJ* and *mamK* mutants of AMB-1 and MSR-1 have led to speculation that additional players may participate in chain formation in a species-specific manner.

AMB-1 contains a homologous copy of *mamK*, called *mamK-like*, within a genomic region termed the magnetosome islet (MIS) (23). The MIS resides outside the MAI and is likely to have been acquired through a secondary horizontal gene transfer event as its genes have differing GC contents and codon usages compared to the MAI (23). The presence of the islet brings up the issue of whether these two different genomic islands, both encoding potential magnetosome proteins, are active in AMB-1. Many of the genes within the MIS are pseudogenes or encode truncated proteins. The only genetic analysis of an MIS gene (*mamE-like*) found that it is not redundant with its MAI homologs and does not play a discernible role in magnetosome formation (24). Additionally, several residues conserved among bacterial actins are absent in MamK-like. In particular, the conserved glutamate residue in its ATPase active site is replaced by an alanine (Fig. 1). In MamK and other actins, the mutation of this glutamate (e.g., E143A in MamK) blocks ATPase activity and filament dynamics both *in vivo* and *in vitro* (6, 20, 21, 25). Previous work has shown that *mamK-like* is expressed *in vivo* (23). Thus, if MamK-like interacts with MamK, it is possible that it would interfere with the dynamics of the chain formation process. These observations raise important issues regarding the functionality of the MIS and the potential involvement of MamK-like in magnetosome chain formation.

While members of different bacterial actin subgroups often coexist in the same organism and carry out their individualized functions without interference from other actin-like proteins, in rare cases, multiple isoforms of the same bacterial actin can also

exist in a single organism. *Bacillus subtilis*, for example, has three forms of MreB, namely, MreB, Mbl (MreB-like), and MreBH (MreB homolog), that promote cell shape by performing related and yet distinct functions in the cell (26–29). Thus, we sought to explore the functionality and potential activity of MamK-like as a partner to MamK in AMB-1. Here, we demonstrate that *mamK-like* has a function in chain alignment in AMB-1. We show that MamK-like interacts with MamK and depends on it for *in vivo* filament formation. Surprisingly, the A141 residue of MamK-like does not block its ATPase activity, allowing the protein to positively participate in MamK filament dynamics *in vivo*. Collectively, we show a unique facet of the process of magnetosome formation and provide evidence that MamK-like modulates MamK activity in AMB-1. Additionally, these findings highlight the diverse manners in which bacteria organize their cellular architectures.

MATERIALS AND METHODS

Growth conditions. AMB-1 mutant strains and those bearing plasmids were grown in a modified MG medium as described previously (17, 30). Cells and culture growth conditions for fluorescence recovery after photobleaching (FRAP) were as described previously (21). Optical densities and coefficient of magnetism (C_{mag}) measurements of strains (measuring the ability of the cells to turn in a magnetic field) in this study are listed in Table S1 in the supplemental material. Media for the yeast two-hybrid (Y2H) strains were prepared according to the TRAFO yeast transformation protocols and previous work (31, 32).

Molecular biology. Plasmids used in this paper are listed in Table S2 in the supplemental material. PCRs were performed with primers listed in Table S3 (Integrated DNA Technologies) and Accuprime *Pfx* DNA polymerase (Invitrogen) on a MyCycler thermocycler (Bio-Rad). Restriction enzymes, calf intestinal phosphatase, and T4 DNA ligase were purchased from New England BioLabs.

Plasmid construction. The markerless Δ*mamK-like* deletion construct was created by PCR of wild-type AMB-1 genomic DNA (gDNA) with the following primers: *NA01* and *NA02* for the upstream recombination site and *NA03* and *NA04* for the downstream recombination site. A fusion PCR using the upstream and downstream fragments as templates was executed using *NA01* and *NA04* primers to generate the deletion insert. The pAK31 plasmid backbone was digested with SpeI enzyme and ligated with the deletion insert, resulting in plasmid pAK576. The pAK576 construct confers resistance to kanamycin and contains the counterselectable marker *sacB*. AMB-1 cells were first selected for kanamycin resistance (the first recombination event). The cells were then counterselected on MG agar with 2% sucrose (the second recombination event). The resulting cells were then screened for the loss of the gene of interest by PCR. The *mamK-like-gfp* plasmid (pAK699) was created by PCR of AMB-1 gDNA with *NA33* and *NA19* primers. The pAK22 plasmid backbone was digested with EcoRI and BamHI enzymes and ligated with the *mamK-like* insertion digested with MfeI and BamHI. The complementation constructs were created by first digesting *mamK-gfp* from the pAK22 backbone with EcoRI and SpeI. Untagged *mamK* (with stop codon) was amplified from AMB-1 gDNA with *NA79* and *NA56* to create pAK742. This construct was then digested with SpeI and SacI and ligated with the *gfp-mamI* insertion amplified from pAK266 with *NA80* and *NA81* to generate pAK726. The pAK726 plasmid was digested with EcoRI and SpeI enzymes and then ligated with the *mamK-like* insertion generated by amplifying AMB-1 gDNA with *NA33* and *NA35* to generate pAK706. To generate the pET-SUMO plasmids for protein expression, the *mamK* and *mamK-like* genes were amplified from AMB-1 gDNA and cloned into a pET-SUMO vector (Invitrogen) following the supplier's protocol. Primers are listed in Table S3 in the supplemental material.

Site-directed mutagenesis. pET-SUMO-*mamK* and pET-SUMO-*mamK-like* plasmids were used as templates for site-directed mutagenesis to create mutants *mamK*^{E143A}, *mamK*^{D17N}, *mamK-like*^{A141E}, and *mamK-like*^{D15N} using a QuikChange II XL site-directed mutagenesis kit (Stratagene). Primers are listed in Table S3 in the supplemental material.

Strain construction. The nonpolar *mamK-like* deletion was constructed in the wild-type and Δ*mamK* backgrounds as described previously (17, 30). Primers used to create the deletion plasmid are listed in Table S3 in the supplemental material. The *mamK mamK-like* double-deletion strain was created by deleting *mamK-like* in a Δ*mamK* background.

Sequence alignment. Accession numbers for the bacterial actin-like proteins used for sequence alignments (Fig. 1) are as follows: for *Magnetospirillum magneticum* AMB-1 MamK-like, ACU87671.1; for *Magnetospirillum magneticum* AMB-1 MamK, YP_420328.1; for *Magnetospirillum gryphiswaldense* MSR-1 MamK, CAM78025.1; for *Thermotoga maritima* MreB, 2WUS_B; and for *Escherichia coli* MreB, EDV65518.1. Alignments were generated with MUSCLE (33).

Western blot analysis of AMB-1. AMB-1 colonies were transferred into 1.5-ml microcentrifuge tubes containing 1.5 ml MG media with 10 μg/ml kanamycin (for plasmid-bearing strains) or MG media alone (for untransformed cells). A 1:100 dilution of AMB-1 cells in 1.5 ml of each culture was inoculated into 10 ml of MG media with or without kanamycin. Cultures were grown in 10% O_2 for 2 days and then passaged at 1:100 into 10 ml of fresh MG medium. These cultures were grown for an additional 2 days, and then cells were harvested by centrifugation (Sorvall Mach 1.6R) at 15,000 × *g* for 15 min at room temperature. Pelleted cells were resuspended in 2× SDS Laemmli buffer (with 5% β-mercaptoethanol). Cells were heated at 70°C for 10 min with mixing at the 5-min mark and loaded onto a 12% Laemmli gel, which was run at 150 V for 1 h. All samples contained roughly equal amounts of cells per volume of 2× SDS Laemmli buffer. Adjustments were based on cell optical density at 400 nm (OD_{400}) (Ultrospec 2100 pro; Amersham Biosciences). Proteins were transferred onto a polyvinylidene difluoride (PVDF) membrane at 100 mA for 1 h. After the membrane was blocked for 1 h at room temperature with 5% milk–TBST (Tris-buffered saline–Tween 20), primary antibody was applied (chicken anti-green fluorescent protein [α-GFP]; Aves no. GFP-1020) (1:5,000) for 1 h at room temperature. After washing with TBST multiple times, secondary antibody (goat anti-chicken conjugated to horseradish peroxidase [HRP]; Aves H-1004) (1:20,000) was applied for 1 h at room temperature. A Western Lightning Plus ECL system (PerkinElmer) was used to visualize bands.

Fluorescence and differential interference contrast microscopy. Light microscopy was carried out using a Zeiss AxioImager M2 microscope equipped with a Qimaging QiClick camera. GFP-tagged proteins were excited by the use of a Lamda LS Illumination system (Sutter Instruments). Images were analyzed with iVision software (Biovision).

FRAP. Agarose pads and slides were prepared as described previously (21). Fluorescence recovery after photobleaching (FRAP) experiments were carried out on a Zeiss 710 UV/visible light (Vis) laser scanning confocal microscope. MamK-GFP filaments were imaged using a 488-nm excitation wavelength at 0.5% to 3.0% laser power. The filaments were bleached using 488-nm laser light at 100% laser power for 7 to 10 iterations. Images were captured every 50 s for up to 30 min through the 100× X oil objective with LSM710 Imaging Software 3.2 (Zeiss). Due to the lack of an autofocus feature, each frame was monitored and manual focusing was performed if necessary. Images were analyzed using Fiji software (34). For each FRAP run, regions of interest (ROIs) were drawn in three areas: (i) the background; (ii) the whole filament; and (iii) the bleached segment. Each whole filament and the bleached ROIs had the background intensity value (arbitrary units) from that time point subtracted. Images that had a steep decrease in fluorescence intensity (generally due to loss of focus rather than photobleaching) were dropped from downstream analysis. To generate percent recovery graphs, runs were normalized by calculating the ratio of bleached ROI intensity to the whole-filament ROI intensity for each time point. The run was considered recovered by the following criteria: (i) the fluorescence intensity of the bleach region returned to 50% of

that measured for the whole filament at the same time point and (ii) the whole-filament fluorescence intensity values did not dip drastically due to photobleaching.

Gene expression analysis. The methods for analysis of gene expression using quantitative reverse transcription-PCR (qRT-PCR) are described in detail in the supplemental material.

Y2H assays. Yeast two-hybrid (Y2H) assays were conducted by employing a previously established plasmid and yeast strain system (32, 35). A set of Y2H plasmids enabled the fusion of proteins of interest via polylinkers to the Gal4 DNA binding (pCD plasmids) or the Gal4 activation domain (pC-ACT plasmids). Gene sequences for *mamK*, *mamK-like*, and *mreB* were amplified from AMB-1 gDNA using primer sets specified in Table S3 in the supplemental material and were ligated into pCD and pC-ACT plasmids through NdeI and BamHI restriction sites. The gene *mamK* was fused to Gal4 domains in pCD.3 and pC-ACT.3, resulting in plasmids pAK140 and pAK141, respectively. The genes *mamK-like* and *mreB* were fused to Gal4 domains in pCD.1 and pC-ACT.1 (for *mamK-like*, pAK485 and pAK483, respectively; for *mreB*, pAK479 and pAK489, respectively). Plasmids were individually transformed into either yeast strain YD116 (mating type **a**) or yeast strain YD119 (mating type α). Cells harboring the pCD and pC-ACT plasmids were created by mating, and cells were selected on medium plates lacking tryptophan and leucine, as genes for their synthesis are carried on the respective plasmids. Mated yeast strains carrying both plasmids were grown in 5 ml of media lacking tryptophan and leucine before volumes were adjusted to ensure that equal numbers of cells (OD_{600} of 0.3) were plated, and then serial 1:10 dilutions were made and plated on plates lacking tryptophan and leucine or lacking tryptophan, leucine, and uracil. Yeast strains YD116 and YD119 utilize the GAL1-URA3 reporter for assessment of Gal4 transcription factor reconstitution upon protein-protein interaction. Hence, the interaction of MamK, MamK-like, and MreB was assessed on plated medium lacking tryptophan, leucine, and uracil. Images were taken using an iPad (Apple).

Expression and purification of MamK and MamK-like. N-terminal tagging of MamK and MamK-like with the SUMO tag allows affinity purification of the proteins and seamless removal of the tag by the action of the SUMO protease. The pET-SUMO plasmids were cotransformed into One Shot *BL21 Star* (*DE3*) chemically competent *Escherichia coli* cells along with the pRARE plasmid carrying several rare tRNAs (36). Transformants were selected on LB medium in the presence of both kanamycin (50 μg/ml) and chloramphenicol (25 μg/ml). For protein expression of either MamK or MamK-like, cells were grown overnight in Terrific Broth (TB) medium in the presence of both antibiotics at 30°C under shaking. Overnight cultures were diluted into fresh medium and grown to OD_{600} ± 0.6 at 37°C; isopropyl β-D-1-thiogalactopyranoside was then added to reach a final concentration of 0.1 mM to induce protein expression, and cultures were incubated with shaking at 16°C overnight. Cells were harvested by centrifugation (7,500 × *g*, 15 min), and the cell pellet was resuspended in 20 mM HEPES (pH 8)–250 mM NaCl. A protease inhibitor cocktail and DNase I were added to the suspension to prevent protein degradation and reduce the viscosity of the lysate, respectively. Cells were disrupted with a French press (1,000 lb/in^2, three passages). The lysate was centrifuged at low speed (10,000 × *g*, 10 min) to remove large debris particles, and the supernatant was ultracentrifuged (150,000 × *g*, 1 h) to separate membranes and polymerized protein from soluble MamK or MamK-like. The supernatant was then loaded onto nickel-nitrilotriacetic acid (Ni-NTA) resin (prepacked 1-ml HisTrap HP column; GE Healthcare) using an Äkta Fast protein liquid chromatography system (GE Healthcare). Three washing steps were carried out with increasing concentrations (20 mM, 50 mM, and 100 mM) of imidazole, and elution was performed at 300 mM imidazole. Eluted proteins were immediately desalted, and the buffer was exchanged using a PD-10 size exclusion chromatography column (stabilization buffer, 100 mM Bis Tris propane; pH 8.5). The seamless removal of the SUMO tag was performed by incubation of the SUMO-tagged proteins with the SUMO protease (the *sumo* gene amplified from *Saccharomyces cerevisiae* and cloned into pET28b was kindly provided by Christopher D. Lima [37]). The incubation mix contained 1 U SUMO protease for 20 μg protein, and proteolysis proceeded for 3 h at 30°C or overnight at 4°C. The proteolysis mixture was loaded onto the nickel affinity column: a successful cleavage of the SUMO tag leaves the untagged protein in the flow-through. The Bradford assay was used for protein quantification.

ATPase activities. The inorganic phosphate release resulting from ATPase activity was measured spectrophotometrically using the Malachite Green test (adapted from reference 38). A 500-μl reaction mixture was prepared in 100 mM Bis-Tris propane buffer (pH 8.5) with known quantities of protein and incubated at room temperature to determine initial velocities. Typically, we used 2 μM protein for ATP concentrations above 1 mM, 4 μM protein at concentrations between 250 μM and 1 mM ATP, and 8 μM at concentrations under 250 μM ATP. The reaction was triggered by addition of ATP and $MgCl_2$ in concentrations ranging from 25 μM to 4 mM. Aliquots (50 μl) were sampled every 5 min, and the reaction was stopped by adding 20 μl of 0.6 M perchloric acid. The colorimetric reaction was made by adding 100 μl of malachite green reagent and 14 μl of a stabilizing solution of 34% sodium citrate. After incubation at room temperature for 10 min using soft stirring, the absorbance was measured at 645 nm in a microplate reader (Tecan Infinite M200). The data were normalized to a standard curve made with phosphate standards prepared in the 100 mM Bis-Tris propane buffer (pH 8.5), and protein-free control reactions were performed.

RESULTS

MamK-like participates in magnetosome chain alignment. In order to investigate the function of MamK-like *in vivo*, we created in-frame deletions of the *mamK-like* gene in wild-type and Δ*mamK* strains. Previous work using RT-PCR had found that *mamK-like* is expressed in wild-type AMB-1 and Δ*mamK* backgrounds (23). Here, we determined using qRT-PCR that *mamK-like* was expressed at approximately half of the levels of *mamK* (see Fig. S1 in the supplemental material). Furthermore, the deletion of *mamK-like* or *mamK* did not result in a change in the expression levels of the other gene (see Fig. S1). Additionally, the deletion of *mamK-like*, alone or in combination with *mamK*, did not result in gross cell morphological changes as assessed by transmission electron microscopy (TEM) (see Fig. S2).

We next investigated if MamK-like is important for the chain-like organization of magnetosomes in AMB-1 cells. To visualize the misalignment of the magnetosome chain, we used a fluorescent fusion to a magnetosome membrane marker (GFP-MamI). In several strains, such as the Δ*mamK*, Δ*mamJ*, Δ*limJ*, and Δ*mamJ* Δ*limJ* mutants, GFP-MamI has been successful in revealing a large range of magnetosome chain organization defects that are congruent with high-resolution imaging via ECT (21, 24, 30). Since it depends on fluorescence microscopy rather than ECT, imaging of GFP-MamI is a rapid and high-throughput method of determining the integrity of the magnetosome chain across a large number of cells in a population. Furthermore, this visualization technique can detect mineral-loaded magnetosomes as well as empty membranes that could otherwise be detected only by ECT. Linear localization patterns of GFP-MamI correlate to aligned magnetosomes (both full and empty), and cells with unaligned magnetosomes have multiple unaligned foci, cell membrane localization, or diffuse staining (Fig. 2B). Compared to wild-type cells that have a high proportion of aligned magnetosomes (77.3%, $n = 1,870$), Δ*mamK* cells display a less organized localization pattern, with only 33.3% of cells showing alignment ($n = 1,161$) (Fig. 2A). The Δ*mamK-like* cells also display a higher degree of disorganization than wild-type cells (45.8% of cells with aligned magnetosomes,

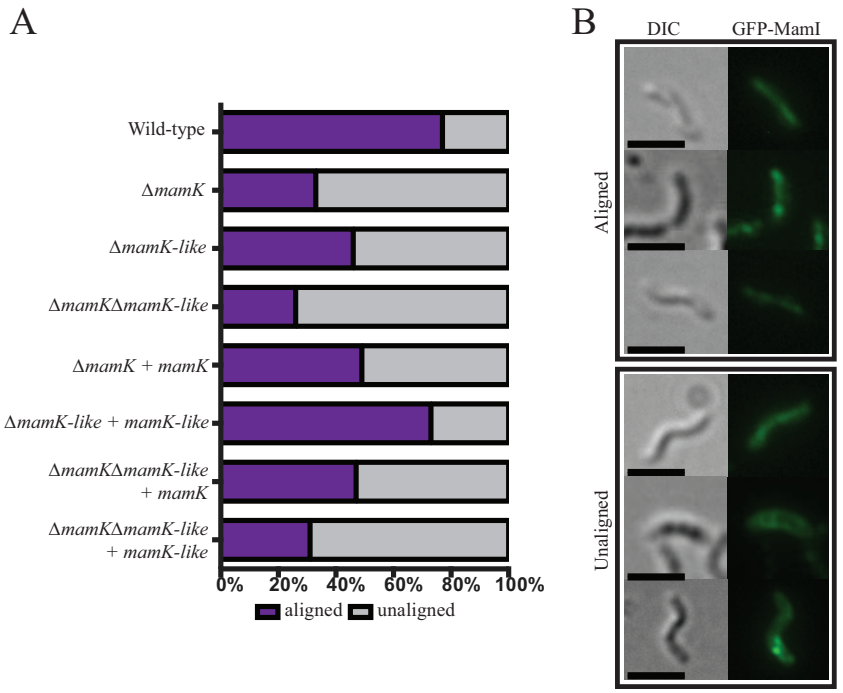

FIG 2 GFP-MamI localization patterns indicate magnetosome alignment. (A) GFP-MamI alone in wild-type (n = 1,870), Δ*mamK* (n = 1,161), Δ*mamK-like* (n = 1,276), and Δ*mamK*Δ*mamK-like* (n = 807) cells. Complementation experiments were performed with GFP-MamI and MamK in Δ*mamK* (n = 685) and Δ*mamK*Δ*mamK-like* (n = 759) cells and with GFP-MamI and MamK-like in Δ*mamK-like* (n = 1,063) and Δ*mamK*Δ*mamK-like* (n = 964) cells. (B) Representative images of aligned localization patterns (linear and linear with puncta) and unaligned localization patterns (diffuse, membrane, and unaligned puncta) are shown. DIC, differential interference contrast. Scale bars = 2 μm.

n = 1,276) (Fig. 2A). The deletion of both *mamK* and *mamK-like* results in the most severe disorganization phenotype (25.8% of cells with aligned magnetosomes, n = 807) (Fig. 2A). Complementation experiments were performed to confirm that these results were due solely to the loss of the targeted gene products. The Δ*mamK* and Δ*mamK-like* cells, as well as the double-deletion cells, were complemented with a copy of the deleted gene on a plasmid. Cells lacking *mamK* were complemented at about 63% of the wild-type level, and cells lacking *mamK-like* were complemented to wild-type levels (Fig. 2A). The differences in complementation levels suggest that protein expression from the plasmid may not be sufficient to completely rescue the Δ*mamK* phenotype. Complementation of the double-deletion strain with either *mamK* or *mamK-like* indicates that the phenotype of this strain is due to gene loss and demonstrates that both MamK and MamK-like participate in chain alignment.

MamK and MamK-like proteins interact in a yeast two-hybrid assay and form colocalizing filaments *in vivo*. MamK-like shares 56% sequence identity with MamK from AMB-1. Given that both proteins are part of the same family, have a high degree of conservation, and participate in the same cellular process, we reasoned that they could potentially interact with each other. In a yeast two-hybrid assay, MamK and MamK-like proteins displayed self-interactions and interactions with each other (Fig. 3). This interaction(s) was specific in that neither MamK nor MamK-like interacted with the more distantly related bacterial actin protein, MreB, from AMB-1, which can interact with itself in the yeast-two hybrid assay (Fig. 3). In negative-control experiments, pairings between empty vector constructs did not result in interaction and growth (Fig. 3). To investigate the potential interactions between these two proteins *in vivo*, we coexpressed MamK-GFP and MamK-like–red fluorescent protein (MamK-like-RFP) and found that they formed colocalizing filaments in AMB-1 (see Fig. S3 in the supplemental material). Taken together, these results suggest that MamK and MamK-like proteins interact in their filamentous forms.

MamK influences MamK-like's ability to form filaments *in vivo*. The results described above indicate that an interaction exists between MamK and MamK-like. We reasoned that formation of filaments of one protein *in vivo* might require the presence of the other. MamK-GFP filaments formed with similar frequencies in wild-type and Δ*mamK-like* strains (data not shown). In contrast, MamK-like-GFP filaments depended on the presence of MamK for efficient filament formation. In the wild-type background, 52% of cells had MamK-like-GFP filaments, 38% of cells had diffuse patterns, and 10% of cells had foci (n = 345) (Fig. 4A). The Δ*mamK-like* background had similar proportions of MamK-like-GFP filaments, with 54% of cells with filaments, 38% with a diffuse pattern, and 8% of cells with foci (n = 441) (Fig. 4A). In contrast, very few cells in the Δ*mamK* (9%) or Δ*mamK* Δ*mamK-like* (6%) background displayed MamK-like-GFP filaments (n = 540 for Δ*mamK* and n = 426 for Δ*mamK* Δ*mamK-like*) (Fig. 4A). To confirm expression of fusion proteins, Western blotting using an anti-GFP antibody was performed on wild-type cells expressing MamK-like-GFP. In contrast to cells expressing MamK-GFP, a distinct signal for the GFP fusion fragment was detected, suggesting that the MamK-like-GFP fusion is less stable than MamK-GFP (Fig. 4C). This may also account for some of the diffuse localization patterns observed in cells expressing MamK-like-GFP (Fig. 4B and C).

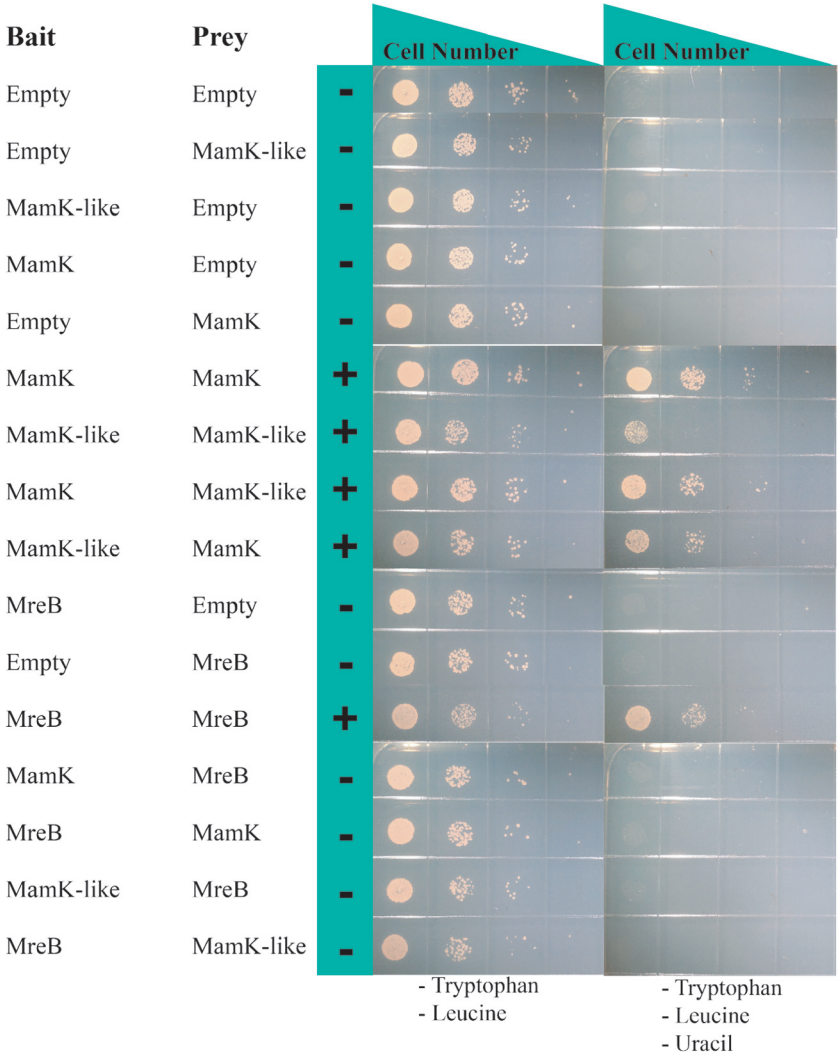

FIG 3 Yeast two-hybrid assays demonstrate interaction between bacterial actin proteins. The results of bait and prey fusions to MamK, MamK-like, and MreB from AMB-1 are shown. Interactions are observed and noted with plus (+) signs, and noninteracting protein pairs are noted with minus (−) signs.

MamK-like can affect MamK turnover *in vivo*. Thus far, our data indicate that MamK and MamK-like are capable of physical and functional interactions within the cell. We previously hypothesized that MamK-like could affect MamK dynamics if the two proteins formed mixed polymers (21) (Fig. 5A). This idea was based on the observations that nucleotide hydrolysis is required for MamK dynamics *in vivo* and that MamK-like carries a mutation that should render it a nonactive ATPase (A141 in MamK-like, corresponding to E143A in MamK) (Fig. 1). The *in vivo* dynamics of MamK have been characterized in previous work with fluorescence recovery after photobleaching (FRAP) assays (21). MamK-GFP filaments localize as thin lines in AMB-1 cells, although, occasionally, curved lines or doubled filaments are also observed (Fig. 5B). During FRAP experiments, sections of GFP-tagged MamK filaments are irreversibly photobleached and the recovery of fluorescence in the bleached segment is tracked over time (Fig. 5C). Recovery in FRAP is most likely the result of monomer turnover (depolymerization/polymerization), filament sliding, or new filament formation events. The half-life ($t_{1/2}$) of recovery denotes the time point at which 50% of the fluorescence intensity returns to the bleached region relative to the whole filament at that same time point. The fluorescence recovery frequency of MamK-GFP has previously been observed in approximately 50% of wild-type cells with a $t_{1/2}$ of 11 ± 6 min (21). In this study, MamK-GFP in the wild-type background had a similar recovery frequency and a slightly higher average $t_{1/2}$ (50% of cells recovered, at a $t_{1/2}$ of 14.3 ± 5.5 min, $n = 32$) (Fig. 5F). The longer recovery times in this set of experiments could be due to the difference in imaging equipment, as less photobleaching occurs with the confocal microscope used in this study, allowing more frequent and longer imaging of cells than in previous work.

Since the two proteins appear to form mixed filaments, we hypothesized that the putative mutations in the ATPase active site of MamK-like could account for the relatively slow dynamics of MamK-GFP filaments and the large proportion of cells in which no recovery is observed. However, the deletion of *mamK-like* did not affect turnover frequency (50%, $n = 22$) or rates of recovery ($t_{1/2}$, 15.5 ± 7.7 min) of MamK-GFP filaments in FRAP experiments (Fig. 5F). In contrast, the total amount of MamK in the cells had an impact on the FRAP experimental results. Loss of endog-

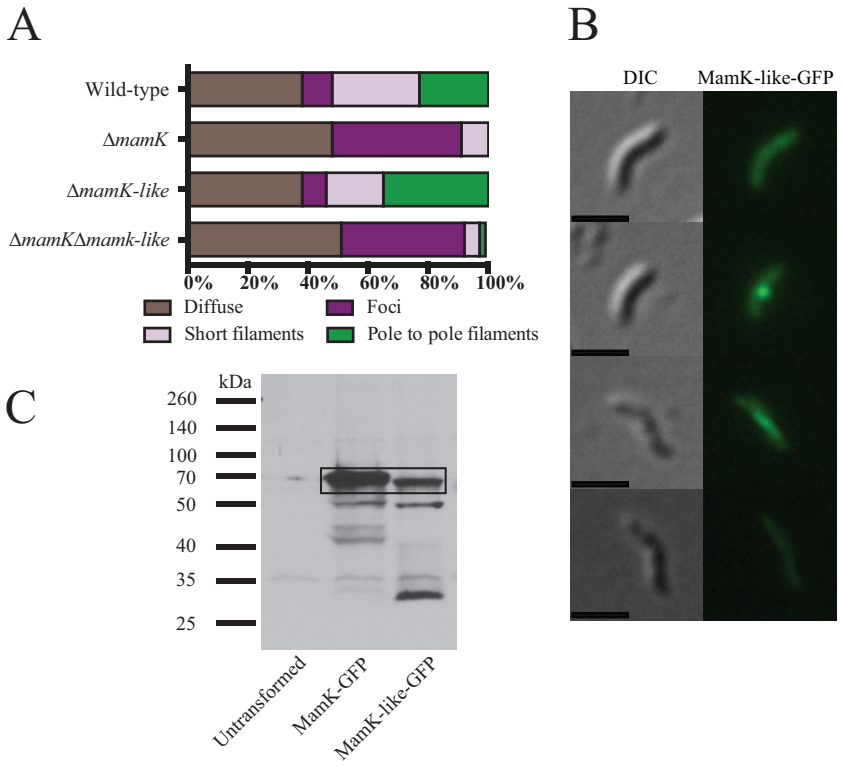

FIG 4 Filament assessment through fluorescent protein fusions. (A) Distribution of MamK-like-GFP localization patterns in AMB-1 cells (wild type $n = 345$, Δ*mamK* $n = 540$, Δ*mamK-like* $n = 441$, and Δ*mamK*Δ*mamK-like* $n = 426$). (B) Representative images of MamK-like-GFP localization patterns of AMB-1 cells with diffuse staining, foci, short filaments, and full-length filaments are shown. Scale bars = 2 μm. (C) A Western blot using anti-GFP antibody detected GFP fusions to MamK (column 2) and MamK-like (column 3) (the box indicates full length) and revealed significant levels of unfused GFP in the MamK-like-GFP expressing cells (column 3).

enous MamK (in the Δ*mamK* background) lowered the recovery frequency (23% of cells recovered compared to 50% of wild-type cells) but did not significantly affect the $t_{1/2}$ of recovering cells (13.2 ± 8.0 min, $n = 44$) (Fig. 5F). However, the $t_{1/2}$s of MamK-GFP filaments in the strain deleted for *mamK* and *mamK-like* were significantly ($P \leq 0.02$; see Fig. S4A in the supplemental material) higher than in Δ*mamK* cells alone (21.2 ± 6.6 min, $n = 45$) (Fig. 5F). Thus, the dynamics of the MamK-GFP filament is most severely impacted when both native MamK and MamK-like are absent. These results show that MamK-like does not have a negative impact on the turnover of MamK filaments *in vivo*. Instead, MamK-like appears to promote the turnover of MamK filaments by supplying a source of monomers in the cytoplasmic pool that are incorporated into MamK filaments, by new filament growth, or by lateral filament sliding. The importance of these potential interactions is most evident when endogenous MamK and MamK-like are absent in the cell.

MamK-like displays ATPase activity despite the E141A mutation. The results described above lead to the surprising conclusion that the interaction of MamK-like with MamK has a positive effect on filament turnover despite the presence of a mutation that should inhibit ATP hydrolysis and as a result impede the depolymerization of filaments. Thus, we investigated whether MamK-like has ATPase activity despite the E141A mutation. Recombinant MamK-like was purified and analyzed in a phosphate release assay. Compared to MamK, which had a K_m of 143 μM and a V_{max} of 0.2 μM $P_i \cdot min^{-1} \cdot uM^{-1}$, MamK-like had a K_m of 127 μM and a V_{max} of 0.32 μM $P_i \cdot min^{-1} \cdot \mu M^{-1}$ in our experiments (Fig. 6). This is surprising, as the substitution of this residue in MamK (Fig. 6) and other actins abolished ATPase activity. When the residue was changed back to a glutamate (A141E), MamK-like displayed a higher level of phosphate release to both MamK and MamK-like, with a K_m of 151 μM and a V_{max} of 0.52 μM $P_i \cdot min^{-1} \cdot uM^{-1}$ (Fig. 6). Additionally, the ATPase activity of MamK-like was abolished when a highly conserved aspartate residue (D15) (Fig. 1) in its phosphate 1 loop, predicted to participate in ATP binding, was mutated (Fig. 6) (39). Combined with the *in vivo* FRAP experiments, these results show that MamK-like is an ATPase that can influence the behavior and function of MamK filaments.

DISCUSSION

The MAI has been the focal point of research on magnetosome formation in recent years. In a scenario that is unusual among MTB, AMB-1 contains a second subset of magnetosome formation genes in the MIS whose function and potential participation in magnetosome formation have been debated. Here, we demonstrate that one gene from the MIS, *mamK-like*, is transcribed and its product interacts with MamK to regulate MamK dynamics and align magnetosomes in the cell.

Magnetosome alignment can be assessed through more than one method. In our research, we used a magnetosome marker for this purpose. Note that, at first glance, whole-cell TEM images (such as those in Fig. S2 in the supplemental material) appear to show no obvious distinctions in magnetosome alignment between

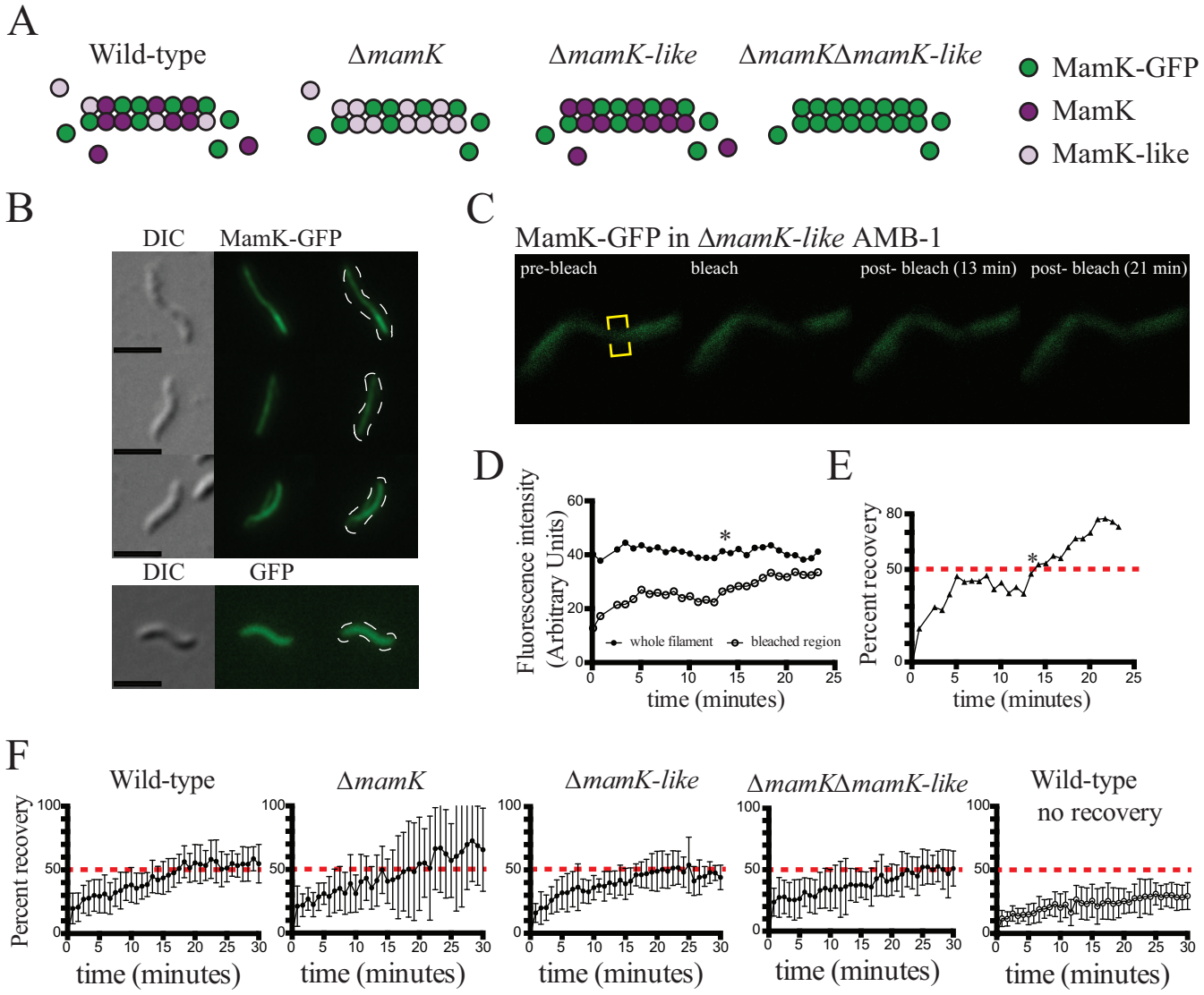

FIG 5 Analysis of MamK-GFP dynamics by fluorescence recovery after photobleaching (FRAP). (A) Schematics representing the types of MamK proteins present in FRAP experiments (green circles, MamK-GFP; dark-purple circles, endogenous MamK; light-purple circles, endogenous MamK-like). (B) DIC and fluorescence images of wild-type AMB-1 cells illustrate MamK-GFP filaments. A cell is shown with cytoplasmic GFP for comparison (bottom panel). Scale bar = 2 μm. (C) A FRAP experiment time course (images are from MamK-GFP in the Δ*mamK-like* background). The panel shows a ×9 zoom of a confocal image—hence the blurred appearance of the filament. Yellow brackets indicate the portion of the MamK-GFP filament designated for photobleaching. (D) Fluorescence intensities of a whole filament (filled circles) and a bleached region (open circles) of the run shown in panel C. (The $t_{1/2}$ is noted by the asterisk at 13 min.) (E) Percent recovery for the same run. (F) Normalized (average ± standard deviation [SD]) percent recovery of each strain's recovering cells. The 50% mark is noted with a dashed red line. Nonrecovering cells (in the wild-type background) are shown for comparison in the last panel.

wild-type and mutant cells. That appearance is misleading, however, since conventional TEM can image only the electron-dense magnetic particles and fails to visualize empty magnetosome membranes. Cells with fragmented chains, for instance, cannot be distinguished from those containing continuous stretches of empty and filled magnetosome membranes. In other words, "gaps" in a wild-type cell are often still filled with empty magnetosomes (as visualized by ECT) whereas gaps in *mamK* deletion cells are truly devoid of any magnetosomes, empty or filled (17). Additionally, in Δ*mamK* mutants, isolated empty magnetosomes have been seen on the side of the cell opposite the magnetosome chain using ECT but not in TEM images (17). This observation could imply that subcellular positioning of an empty magnetosome influences its ability to transport iron or initiate crystal formation. For these reasons, we have developed GFP-MamI as a robust fluorescent marker for magnetosome membranes. By examining various mutants, we have found that this reporter can mark empty and filled magnetosomes and provide a view of chain organization that is consistent with ECT imaging (21, 30).

Using GFP-MamI as a reporter, we find that both MamK and MamK-like are needed to align magnetosomes in AMB-1. Since a higher proportion of Δ*mamK* cells than Δ*mamK-like* cells have misaligned chains, we hypothesize that MamK may be a dominant player in magnetosome chain formation in AMB-1. Consistent with this view, the loss of MamK correlates with the decreased capability of MamK-like-GFP to form filaments whereas MamK-

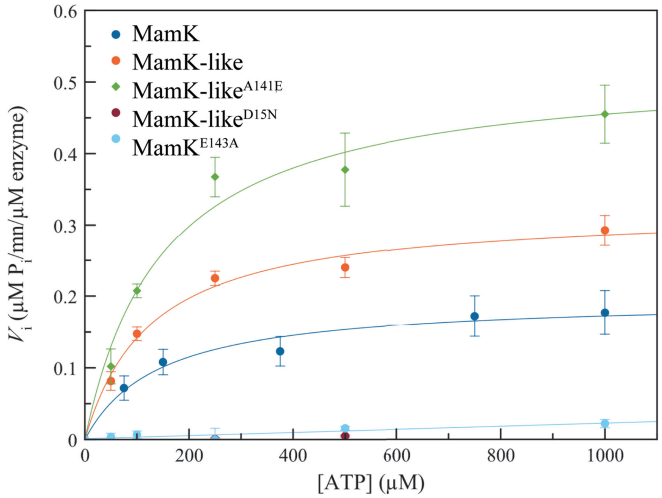

FIG 6 Phosphate release assays indicate an ATPase activity for MamK-like. MamK, MamK-like, MamK-like^{A141E}, MamK-like^{D15N}, and MamK^{E143A} were assayed for phosphate release.

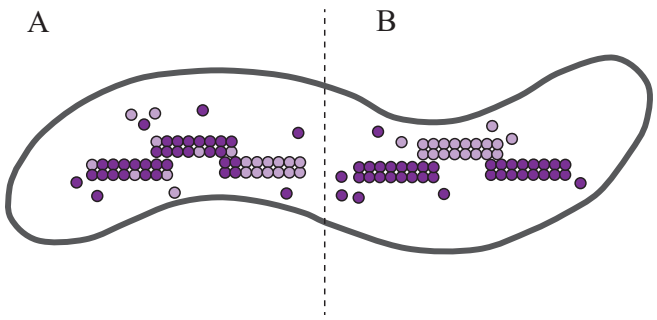

FIG 7 Possible modes for MamK/MamK-like interaction. (A) Interchangeable monomers of MamK (dark-purple circles) and MamK-like (light-purple circles) were incorporated into a copolymer filament. Additionally, MamK may serve as a nucleating protein for MamK-like. (B) MamK filaments serve as nucleating sites for MamK-like filaments to form via lateral association.

like has no influence on the ability of MamK-GFP to form filaments in AMB-1 (N. Abreu, unpublished data). Previously, expression of MamK-like, fused to a fluorescent protein, in *E. coli* allowed the formation of filaments that resemble those seen in AMB-1 (23). Since MamK was not present in those *E. coli* strains, it is possible that overexpression of MamK-like can override the requirement of MamK for robust filament formation. Unfortunately, to date we have been unable to generate antibodies that unambiguously distinguish between MamK and MamK-like, thus making it difficult to directly measure the endogenous protein levels.

Perhaps the most surprising of our results is that MamK-like can hydrolyze ATP. The substitution at residue 141 of MamK-like (A141 in MamK-like and E143 in MamK) should abolish ATP hydrolysis since that site coordinates ATP through a Mg^{2+} ion in both eukaryotic and bacterial actins (39). The absence of the glutamate residue is not the only feature that distinguishes MamK-like from other actins. The so-called "phosphate 1" (DLGT) and "adenosine" glycine-rich loop (GGG) regions, highly conserved in the actin-like family and involved in ATP phosphates binding, are also modified in MamK-like (with DFGY and GAG, respectively) (Fig. 1) (39). Despite these changes, MamK-like is still capable of hydrolyzing ATP *in vitro*, a finding that is consistent with its positive role in promoting MamK filament dynamics *in vivo*. This suggests that several modifications of the ATPase active site are compensating for the loss of the glutamate at position 141. Determining the mechanistic basis of MamK-like's ATPase activity will be an important addition to our knowledge of the structural diversity and evolution of bacterial actins.

Given the data in this study, some potential scenarios can be envisioned to explain how MamK and MamK-like behave in AMB-1. Because MamK influences MamK-like-GFP filament formation *in vivo* (Fig. 4) and because the two proteins colocalize (see Fig. S3 in the supplemental material) and are able to interact with each other (Fig. 3), we would hypothesize that they either form a mixed copolymer (Fig. 7A) or are interacting laterally as pure filaments (Fig. 7B). In the copolymer mode of interaction, MamK and MamK-like proteins would form an interchangeable monomer pool whose total concentration is the most important determinant of efficient filament dynamics. Thus, the most severe phenotypes are observed when both proteins are absent from the cell. If monomers cannot mix, pure MamK filaments would then serve as nucleating sites for MamK-like to form filaments via lateral association. In this case, the dynamics seen in FRAP can be due to sliding of filaments against each other. In the double-deletion strain, the total number of filaments falls below the threshold required for efficient filament sliding and recovery in FRAP.

While our current experimental techniques do not provide sufficient resolution to unequivocally distinguish between these two modes of interaction, we believe that the simplest scenario to explain all of the data is the formation of mixed filaments between MamK and MamK-like. This view is partly influenced by the observation that recovery in FRAP experiments is dependent on the ATPase activity of MamK. Since ATPase activity is required for the *in vitro* depolymerization of MamK filaments (20) and of those of all actin-like proteins examined to date (6, 20, 21, 25), it is likely that recovery in FRAP is due to polymerization/depolymerization events rather than filament sliding. Furthermore, an examination of a structural model of MamK and its homology to MamK-like indicate that individual monomers of these two proteins could interact at critical points of contact. Previous structural analysis of MreB from *Thermotoga maritima* identified potential contact points that link monomers to one another in a protofilament (Fig. 1, marked pink) (40). A model of MamK monomers, based on this *Thermotoga maritima* MreB structure, fit within the filament structure of MamK, obtained by electron microscopy, with high confidence (20). In a multiple-sequence alignment, many of the residues in these points of contact are conserved between diverse MreB proteins (Fig. 1, marked blue). Similarly, these regions are conserved between MamK and MamK-like (Fig. 1, marked green) but distinct from MreB. MamK and MamK-like also share a 5-residue region, unique to the MamK family, that is predicted to be important for protofilaments to form double-stranded filaments (Fig. 1, red box) (20). These comparisons indicate that MamK and MamK-like have the necessary sequence conservation to form a mixed copolymer. Additionally, the variations in these putative contact sites between MamK and MreB may prevent unwanted cross talk between functionally distinct families of bacterial actins that have to coexist in the same cell.

The coexistence and cooperation between MamK and MamK-

like are reminiscent of presence of multiple MreB isoforms in *B. subtilis*, which partner in cell shape determination (27, 28, 41). The existence of multiple MamK isoforms within the same cell is not limited to AMB-1, however. The alphaproteobacterium *Magnetovibrio blakemorei* MV-1, as well as gammaproteobacterium strain SS-5, contains two MamK homologs within its MAIs (42). In contrast to MamK-like, however, these MamKs have normal ATPase active sites (N. Abreu and A. Komeili, unpublished data). Additionally, the magnetotactic deltaproteobacteria, such as *Desulfovibrio magneticus* RS-1 and *Desulfamplus magnetomortis* BW-1, contain MamK as well as another potential bacterial actin-like protein, Mad28, within their MAIs (43). While Mad28 is not part of the MamK subfamily, it is possible that it participates in chain alignment through interactions with MamK. As more magnetotactic bacterial genomes are sequenced, we may find that participation between multiple MamK family members is a rather common mode of magnetosome chain organization.

Finally, studies on the interactions and dynamics of MamK and its homologs can have broader implications in the understanding of the evolution and diversity of the vastly understudied superfamily of bacterial actins. In most eukaryotes, actin is highly conserved and its function and dynamics are impacted by a standard set of actin binding proteins. Interestingly, the intestinal parasite *Giardia intestinalis* contains one of the most divergent eukaryotic actins and also lacks many of the canonical actin binding proteins (44). This fascinating "exception to the rule" supports a hypothesis that preservation of essential interactions between actin and its conserved regulatory partners is a key evolutionary constraint that limits the protein's sequence divergence among eukaryotes. In contrast, the various families of bacterial actins are highly divergent at the sequence level, indicating the absence of a common set of binding proteins and regulators for these proteins. In such a system, isoforms of a bacterial actin-like protein with variations in ATPase activity or binding capacity can provide a rapid path for incorporation of regulatory modules within the cell.

ACKNOWLEDGMENTS

We thank members of the Komeili laboratory for their critical reading and assessment of the manuscript. We also thank Sandra Préveral and Catherine Brutesco in the Pignol Laboratory for their assistance in gene expression and site-directed mutagenesis. Additionally, we thank the members of the Zambryski laboratory for plasmids and antibodies given for this study. Additionally, the equipment and, in particular, the assistance of Steve Ruzin and Denise Schichnes at the UC Berkeley College of Natural Resources Biological Imaging Facility (NIH 1S10RR026866-01) were instrumental for this work.

N.A. is funded through the UC Berkeley Chancellor's fellowship, a UC Berkeley Mentored Research award, and the American Society for Microbiology Robert D. Watkins Fellowship. A.K. is supported by the National Institutes of Health (R01GM084122).

REFERENCES

1. **Cornejo E, Abreu N, Komeili A.** 2014. Compartmentalization and organelle formation in bacteria. Curr. Opin. Cell Biol. **26:**132–138. http://dx.doi.org/10.1016/j.ceb.2013.12.007.
2. **Murat D, Byrne M, Komeili A.** 2010. Cell biology of prokaryotic organelles. Cold Spring Harb. Perspect. Biol. **2:**a000422. http://dx.doi.org/10.1101/cshperspect.a000422.
3. **Savage DF, Afonso B, Chen AH, Silver PA.** 2010. Spatially ordered dynamics of the bacterial carbon fixation machinery. Science **327:**1258–1261. http://dx.doi.org/10.1126/science.1186090.
4. **Balkwill DL, Maratea D, Blakemore RP.** 1980. Ultrastructure of a magnetotactic spirillum. J. Bacteriol. **141:**1399–1408.
5. **Frankel RB, Bazylinski DA, Johnson MS, Taylor BL.** 1997. Magneto-aerotaxis in marine coccoid bacteria. Biophys. J. **73:**994–1000. http://dx.doi.org/10.1016/S0006-3495(97)78132-3.
6. **Derman AI, Becker EC, Truong BD, Fujioka A, Tucey TM, Erb ML, Patterson PC, Pogliano J.** 2009. Phylogenetic analysis identifies many uncharacterized actin-like proteins (Alps) in bacteria: regulated polymerization, dynamic instability and treadmilling in Alp7A. Mol. Microbiol. **73:**534–552. http://dx.doi.org/10.1111/j.1365-2958.2009.06771.x.
7. **Ozyamak E, Kollman JM, Komeili A.** 2013. Bacterial actins and their diversity. Biochemistry **52:**6928–6939. http://dx.doi.org/10.1021/bi4010792.
8. **Jones LJ, Carballido-López R, Errington J.** 2001. Control of cell shape in bacteria: helical, actin-like filaments in Bacillus subtilis. Cell **104:**913–922. http://dx.doi.org/10.1016/S0092-8674(01)00287-2.
9. **Domínguez-Escobar J, Chastanet A, Crevenna AH, Fromion V, Wedlich-Söldner R, Carballido-López R.** 2011. Processive movement of MreB-associated cell wall biosynthetic complexes in bacteria. Science **333:**225–228. http://dx.doi.org/10.1126/science.1203466.
10. **Garner EC, Bernard R, Wang W, Zhuang X, Rudner DZ, Mitchison T.** 2011. Coupled, circumferential motions of the cell wall synthesis machinery and MreB filaments in B. subtilis. Science **333:**222–225. http://dx.doi.org/10.1126/science.1203285.
11. **Mauriello EMF, Mouhamar F, Nan B, Ducret A, Dai D, Zusman DR, Mignot T.** 2010. Bacterial motility complexes require the actin-like protein, MreB and the Ras homologue, MglA. EMBO J. **29:**315–326. http://dx.doi.org/10.1038/emboj.2009.356.
12. **Jensen RB, Gerdes K.** 1997. Partitioning of plasmid R1. The ParM protein exhibits ATPase activity and interacts with the centromere-like ParR-parC complex. J. Mol. Biol. **269:**505–513.
13. **Møller-Jensen J, Borch J, Dam M, Jensen RB, Roepstorff P, Gerdes K.** 2003. Bacterial mitosis: ParM of plasmid R1 moves plasmid DNA by an actin-like insertional polymerization mechanism. Mol. Cell **12:**1477–1487. http://dx.doi.org/10.1016/S1097-2765(03)00451-9.
14. **Gayathri P, Fujii T, Møller-Jensen J, van den Ent F, Namba K, Löwe J.** 2012. A bipolar spindle of antiparallel ParM filaments drives bacterial plasmid segregation. Science **338:**1334–1337. http://dx.doi.org/10.1126/science.1229091.
15. **Lara B, Rico AI, Petruzzelli S, Santona A, Dumas J, Biton J, Vicente M, Mingorance J, Massidda O.** 2005. Cell division in cocci: localization and properties of the Streptococcus pneumoniae FtsA protein. Mol. Microbiol. **55:**699–711. http://dx.doi.org/10.1111/j.1365-2958.2004.04432.x.
16. **Szwedziak P, Wang Q, Freund SM, Löwe J.** 2012. FtsA forms actin-like protofilaments. EMBO J. **31:**2249–2260. http://dx.doi.org/10.1038/emboj.2012.76.
17. **Komeili A, Li Z, Newman DK, Jensen GJ.** 2006. Magnetosomes are cell membrane invaginations organized by the actin-like protein MamK. Science **311:**242–245. http://dx.doi.org/10.1126/science.1123231.
18. **Katzmann E, Müller FD, Lang C, Messerer M, Winklhofer M, Plitzko JM, Schüler D.** 2011. Magnetosome chains are recruited to cellular division sites and split by asymmetric septation. Mol. Microbiol. **82:**1316–1329. http://dx.doi.org/10.1111/j.1365-2958.2011.07874.x.
19. **Philippe N, Wu L-F.** 2010. An MCP-like protein interacts with the MamK cytoskeleton and is involved in magnetotaxis in Magnetospirillum magneticum AMB-1. J. Mol. Biol. **400:**309–322. http://dx.doi.org/10.1016/j.jmb.2010.05.011.
20. **Ozyamak E, Kollman J, Agard DA, Komeili A.** 2013. The bacterial actin MamK: in vitro assembly behavior and filament architecture. J. Biol. Chem. **288:**4265–4277. http://dx.doi.org/10.1074/jbc.M112.417030.
21. **Draper O, Byrne ME, Li Z, Keyhani S, Barrozo JC, Jensen G, Komeili A.** 2011. MamK, a bacterial actin, forms dynamic filaments in vivo that are regulated by the acidic proteins MamJ and LimJ. Mol. Microbiol. **82:**342–354. http://dx.doi.org/10.1111/j.1365-2958.2011.07815.x.
22. **Scheffel A, Gruska M, Faivre D, Linaroudis A, Plitzko JM, Schüler D.** 2006. An acidic protein aligns magnetosomes along a filamentous structure in magnetotactic bacteria. Nature **440:**110–114. http://dx.doi.org/10.1038/nature04382.
23. **Rioux J-B, Philippe N, Pereira S, Pignol D, Wu L-F, Ginet N.** 2010. A second actin-like MamK protein in Magnetospirillum magneticum AMB-1 encoded outside the genomic magnetosome island. PLoS One **5:**e9151. http://dx.doi.org/10.1371/journal.pone.0009151.
24. **Quinlan A, Murat D, Vali H, Komeili A.** 2011. The HtrA/DegP family protease MamE is a bifunctional protein with roles in magnetosome protein localization and magnetite biomineralization. Mol. Microbiol. **80:**1075–1087. http://dx.doi.org/10.1111/j.1365-2958.2011.07631.x.

25. **Garner EC, Campbell CS, Mullins RD.** 2004. Dynamic instability in a DNA-segregating prokaryotic actin homolog. Science **306:**1021–1025. http://dx.doi.org/10.1126/science.1101313.
26. **Carballido-López R, Formstone A, Li Y, Ehrlich SD, Noirot P, Errington J.** 2006. Actin homolog MreBH governs cell morphogenesis by localization of the cell wall hydrolase LytE. Dev. Cell **11:**399–409. http://dx.doi.org/10.1016/j.devcel.2006.07.017.
27. **Kawai Y, Asai K, Errington J.** 2009. Partial functional redundancy of MreB isoforms, MreB, Mbl and MreBH, in cell morphogenesis of Bacillus subtilis. Mol. Microbiol. **73:**719–731. http://dx.doi.org/10.1111/j.1365-2958.2009.06805.x.
28. **Soufo HJD, Graumann PL.** 2003. Actin-like proteins MreB and Mbl from Bacillus subtilis are required for bipolar positioning of replication origins. Curr. Biol. **13:**1916–1920. http://dx.doi.org/10.1016/j.cub.2003.10.024.
29. **Domínguez-Cuevas P, Porcelli I, Daniel RA, Errington J.** 2013. Differentiated roles for MreB-actin isologues and autolytic enzymes in Bacillus subtilis morphogenesis. Mol. Microbiol. **89:**1084–1098. http://dx.doi.org/10.1111/mmi.12335.
30. **Murat D, Quinlan A, Vali H, Komeili A.** 2010. Comprehensive genetic dissection of the magnetosome gene island reveals the step-wise assembly of a prokaryotic organelle. Proc. Natl. Acad. Sci. U. S. A. **107:**5593–5598. http://dx.doi.org/10.1073/pnas.0914439107.
31. **Schiestl R, Gietz D.** 1989. High efficiency transformation of intact yeast cells using single stranded nucleic acids as a carrier. Curr. Genet. **16:**339–346. http://dx.doi.org/10.1007/BF00340712.
32. **Durfee T, Draper O, Zupan J, Conklin DS, Zambryski PC.** 1999. New tools for protein linkage mapping and general two-hybrid screening. Yeast **15:**1761–1768. http://dx.doi.org/10.1002/(SICI)1097-0061(199912)15:16<1761::AID-YEA494>3.0.CO;2-C.
33. **Edgar RC.** 2004. MUSCLE: multiple sequence alignment with high accuracy and high throughput. Nucleic Acids Res. **32:**1792–1797. http://dx.doi.org/10.1093/nar/gkh340.
34. **Schindelin J, Arganda-Carreras I, Frise E, Kaynig V, Longhair M, Pietzsch T, Preibisch S, Rueden C, Saalfeld S, Schmid B, Tinevez J-Y, White DJ, Hartenstein V, Eliceiri K, Tomancak P, Cardona A.** 2012. Fiji: an open-source platform for biological-image analysis. Nat. Methods **9:**676–682. http://dx.doi.org/10.1038/nmeth.2019.
35. **Ward DV, Draper O, Zupan JR, Zambryski PC.** 2002. Peptide linkage mapping of the Agrobacterium tumefaciens vir-encoded type IV secretion system reveals protein subassemblies. Proc. Natl. Acad. Sci. U. S. A. **99:**11493–11500. http://dx.doi.org/10.1073/pnas.172390299.
36. **Rogulin EA, Perevyazova TA, Zheleznaya LA, Matvienko NI.** 2004. Plasmid pRARE as a vector for cloning to construct a superproducer of the site-specific nickase N.BspD6I. Biochemistry (Mosc) **69:**1123–1127. http://dx.doi.org/10.1023/B:BIRY.0000046886.19428.d5.
37. **Mossessova E, Lima CD.** 2000. Ulp1-SUMO crystal structure and genetic analysis reveal conserved interactions and a regulatory element essential for cell growth in yeast. Mol. Cell **5:**865–876. http://dx.doi.org/10.1016/S1097-2765(00)80326-3.
38. **Lanzetta PA, Alvarez LJ, Reinach PS, Candia OA.** 1979. An improved assay for nanomole amounts of inorganic phosphate. Anal. Biochem. **100:**95–97. http://dx.doi.org/10.1016/0003-2697(79)90115-5.
39. **Bork P, Sander C, Valencia A.** 1992. An ATPase domain common to prokaryotic cell cycle proteins, sugar kinases, actin, and hsp70 heat shock proteins. Proc. Natl. Acad. Sci. U. S. A. **89:**7290–7294. http://dx.doi.org/10.1073/pnas.89.16.7290.
40. **van den Ent F, Amos LA, Löwe J.** 2001. Prokaryotic origin of the actin cytoskeleton. Nature **413:**39–44. http://dx.doi.org/10.1038/35092500.
41. **Heichlinger A, Ammelburg M, KleinschnitzE-M, Latus A, Maldener I, Flärdh K, Wohlleben W, Muth G.** 2011. The MreB-like protein Mbl of Streptomyces coelicolor A3(2) depends on MreB for proper localization and contributes to spore wall synthesis. J. Bacteriol. **193:**1533–1542. http://dx.doi.org/10.1128/JB.01100-10.
42. **Jogler C, Kube M, Schübbe S, Ullrich S, Teeling H, Bazylinski DA, Reinhardt R, Schüler D.** 2009. Comparative analysis of magnetosome gene clusters in magnetotactic bacteria provides further evidence for horizontal gene transfer. Environ. Microbiol. **11:**1267–1277. http://dx.doi.org/10.1111/j.1462-2920.2009.01854.x.
43. **Lefèvre CT, Trubitsyn D, Abreu F, Kolinko S, Jogler C, de Almeida LGP, de Vasconcelos ATR, Kube M, Reinhardt R, Lins U, Pignol D, Schüler D, Bazylinski DA, Ginet N.** 2013. Comparative genomic analysis of magnetotactic bacteria from the Deltaproteobacteria provides new insights into magnetite and greigite magnetosome genes required for magnetotaxis. Environ. Microbiol. **15:**2712–2735. http://dx.doi.org/10.1111/1462-2920.12128.
44. **Paredez AR, Assaf ZJ, Sept D, Timofejeva L, Dawson SC, Wang C- JR, Cande WZ.** 2011. An actin cytoskeleton with evolutionarily conserved functions in the absence of canonical actin-binding proteins. Proc. Natl. Acad. Sci. U. S. A. **108:**6151–6156. http://dx.doi.org/10.1073/pnas.1018593108.